Signals from intra-abdominal fat modulate insulin and leptin sensitivity through different mechanisms: Neuronal involvement in food-intake regulation

Tetsuya Yamada,[1,7] Hideki Katagiri,[2,7,*] Yasushi Ishigaki,[1,7] Takehide Ogihara,[2] Junta Imai,[1,2] Kenji Uno,[1,2] Yutaka Hasegawa,[1,2] Junhong Gao,[1,2] Hisamitsu Ishihara,[1] Akira Niijima,[3] Hiroyuki Mano,[4] Hiroyuki Aburatani,[5] Tomoichiro Asano,[6] and Yoshitomo Oka[1]

[1] Division of Molecular Metabolism and Diabetes
[2] Division of Advanced Therapeutics for Metabolic Diseases, Center for Translational and Advanced Animal Research
Tohoku University Graduate School of Medicine, Sendai 980-8575, Japan
[3] Niigata University School of Medicine, Niigata 951-8150, Japan
[4] Division of Functional Genomics, Jichi Medical School, Kawachi-gun, Tochigi 329-0498, Japan
[5] Research Center for Advanced Science and Technology, University of Tokyo, Tokyo 153-8904, Japan
[6] Department of Physiological Chemistry and Metabolism, University of Tokyo, Tokyo 113-8655, Japan
[7] These authors contributed equally to this work.
*Correspondence: katagiri-tky@umin.ac.jp

Summary

Intra-abdominal fat accumulation is involved in development of the metabolic syndrome, which is associated with insulin and leptin resistance. We show here that ectopic expression of very low levels of uncoupling protein 1 (UCP1) in epididymal fat (Epi) reverses both insulin and leptin resistance. UCP1 expression in Epi improved glucose tolerance and decreased food intake in both diet-induced and genetically obese mouse models. In contrast, UCP1 expression in Epi of leptin-receptor mutant mice did not alter food intake, though it significantly decreased blood glucose and insulin levels. Thus, hypophagia induction requires a leptin signal, while the improved insulin sensitivity appears to be leptin independent. In wild-type mice, local-nerve dissection in the epididymis or pharmacological afferent blockade blunted the decrease in food intake, suggesting that afferent-nerve signals from intra-abdominal fat tissue regulate food intake by modulating hypothalamic leptin sensitivity. These novel signals are potential therapeutic targets for the metabolic syndrome.

Introduction

The explosive increase in obesity has become a major public health concern in most industrialized countries (Flier, 2004; Friedman, 2003). Insulin resistance is a fundamental contributor to the metabolic syndrome associated with type 2 diabetes, hypertension, hyperlipidemia, and atherosclerosis. Major advancements in this field include the discoveries of adipocyte-derived humoral factors, such as leptin (Friedman and Halaas, 1998). Leptin conveys energy-storage information from adipose tissue to the central nervous system, leading to food-intake suppression. However, in patients with ordinary obesity, serum leptin levels are increased in proportion to body fat (Considine et al., 1996), but the responses to leptin are impaired (Heymsfield et al., 1999), which defines a state of leptin resistance. Leptin resistance also contributes to the development of obesity and obesity-related metabolic disorders.

Fat accumulation in intra-abdominal fat tissue is involved in development of the metabolic syndrome (Bjorntorp, 1992; Matsuzawa et al., 1995) associated with insulin and leptin resistance (Friedman, 2003). Therefore, in this study, to examine whether the metabolic changes in intra-abdominal fat tissue affect insulin and leptin resistance as well as systemic glucose metabolism, we attempted to express uncoupling protein 1 (UCP1), which functions to dissipate energy as heat (Klingenberg and Huang, 1999), in epididymal fat tissue (Epi) in mice with obesity and diabetes.

Results and discussion

C57BL/6 mice were subjected to direct injection of the UCP1 adenovirus vector into Epi (UCP1 mice) after the development of diabetes associated with obesity in response to high-fat chow preloading for 4 weeks. Mice given the LacZ adenovirus were used as controls (LacZ mice). Immunoblotting detected adenovirus-mediated UCP1 expression in Epi (see Figure S1A in the Supplemental Data available with this article online), and this expression was restricted to Epi (Fig. S1A). UCP1 expression in Epi was detectable on the first day after adenoviral injection and was increased on day 3 but had fallen to very low levels by day 7 (Figure S1B). However, expression levels were far below those of endogenous protein in BAT: on day 3, approximately 5% per unit weight protein (Figure S1B). UCP1 expression was restricted to very limited portions of the tissue (left panel of Figure 1B). Judging from the intensity of immunostaining, UCP1 expression levels in UCP1-expressing white adipocytes did not reach those in brown adipocytes (right panel of Figure 1B). UCP1-expressing adipocytes were significantly smaller than UCP1-nonexpressing adipocytes in the same tissue (Figure 1C), suggesting enhanced metabolism in the former.

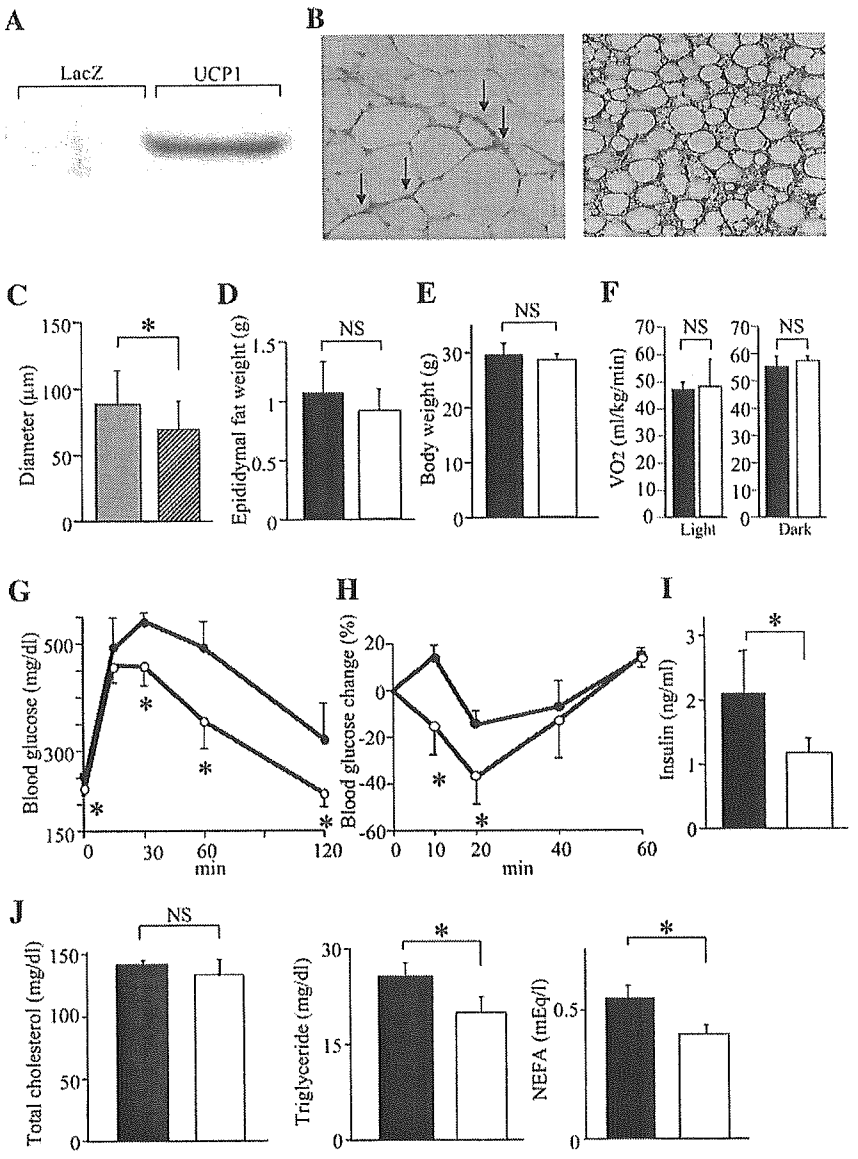

Figure 1. UCP1 expression in Epi improved glucose tolerance and insulin sensitivity

A) Immunoblotting, with anti-UCP1 antibody, of Epi extracts from LacZ and UCP1 mice on day 3 after adenoviral administration.

B) Immunohistochemistry, with anti-UCP1 antibody, of Epi (left panel) and BAT (right panel) sections from a UCP1 mouse on day 3 after adenoviral administration. These two samples were immunostained under the same conditions.

C) Diameters of UCP1-nonexpressing (gray bar) and UCP1-expressing (hatched bar) adipocytes in Epi from UCP1 mice on day 3 after adenoviral administration.

D–J) Epididymal fat weights (**D**), body weights (**E**), resting oxygen consumption during light and dark phase (**F**), and metabolic parameters (**G–J**) of LacZ mice (black bars) and UCP1 mice (white bars) on day 3 after adenoviral administration. Glucose-tolerance (**G**) and insulin-tolerance tests (**H**) were performed on day 3. Data in (**H**) are expressed as percentages of the blood glucose levels immediately before intraperitoneal insulin loading. Serum insulin levels (**I**) and serum lipid parameters ([**J**]; left: total cholesterol, middle: triglyceride, right: free fatty acids) were measured after a 10 hr fast (n = 6 per group). Data are presented as means ± SD (n = 6 per group). *$p < 0.05$ by unpaired t test.

We further confirmed enhanced metabolism by adenoviral UCP1 expression using 3T3-L1 adipocytes. UCP1 expression decreased intracellular ATP concentrations (Figure S1C) and increased levels of peroxisome proliferator-activated receptor γ coactivator (PGC) 1α and cytochrome c expression (Figure S1D). Thus, exogenous UCP1 was functionally active, resulting in increased mitochondrial biosynthesis in adipocytes.

However, neither total Epi weights nor body weights differed between LacZ and UCP1 mice on day 3 after adenoviral administration (Figures 1D and 1E). Oxygen consumption was not affected by UCP1 expression in Epi during either the light or the dark phase (Figure 1F), also reflecting the very limited UCP1 expression. Therefore, to avoid the secondary effects of body-weight change, we analyzed metabolic parameters on day 3. To our surprise, however, even very limited UCP1 expression in Epi resulted in marked changes in metabolic phenotype.

Glucose- and insulin-tolerance tests indicated marked improvements in glucose tolerance and insulin sensitivity (Figures 1G and 1H). Fasting blood glucose (Figure 1G) and insulin (Figure 1I) levels were significantly lower in UCP1 mice, further confirming improved insulin sensitivity. In addition, serum lipid parameters, including triglycerides and free fatty acids (Figure 1J), were also improved with UCP1 expression in Epi. Thus, limited regional expression of UCP1 in Epi markedly improved systemic insulin resistance, resulting in improvement of diabetes and dyslipidemia.

Next, we measured serum adipocytokine levels (Figure 2A). Adiponectin and tumor necrosis factor α levels were not significantly altered. In contrast, serum leptin was markedly decreased, by 46%, with UCP1 expression in Epi. Although intra-abdominal fat-tissue weights were unaltered or only very slightly decreased in UCP1 mice (Figure 1D and Figure S1E),

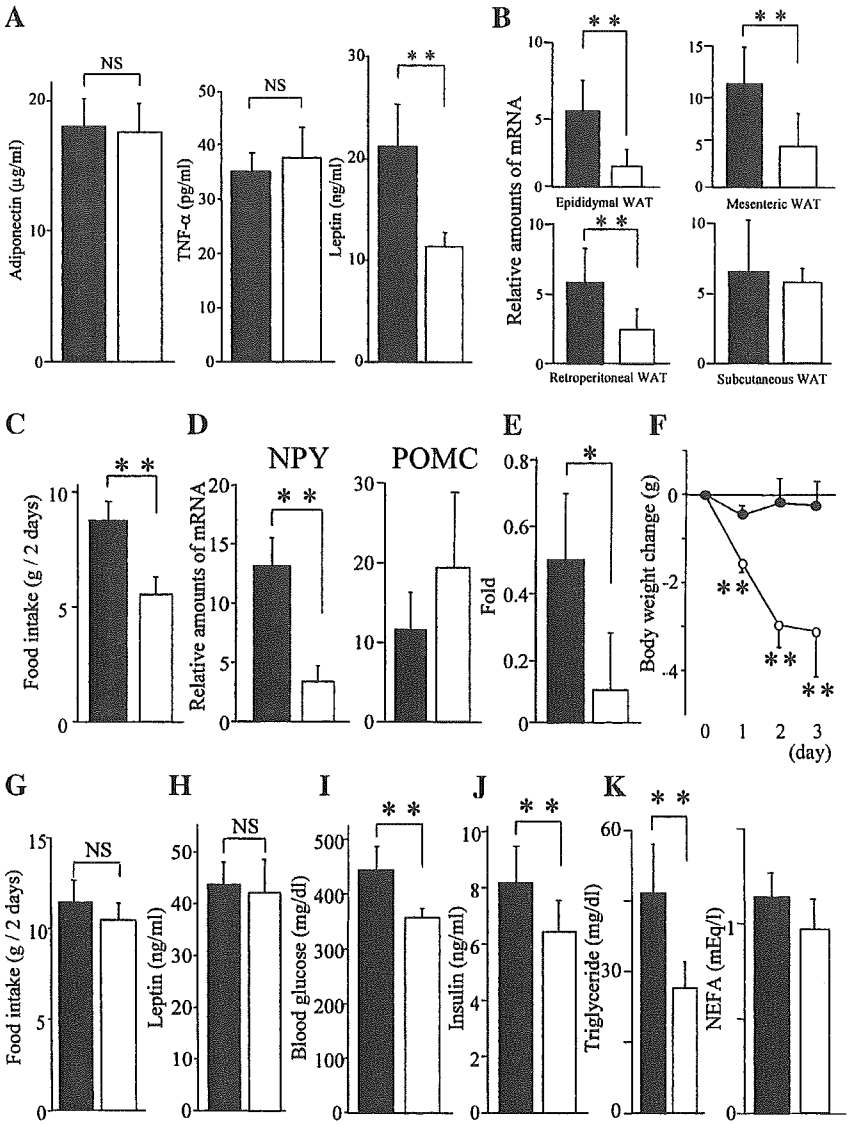

Figure 2. UCP1 expression in Epi improved leptin sensitivity

A–F) LacZ (black bars) or UCP1 (white bars) adenovirus was injected into Epi of mice with dietary obesity.

A) Serum adipocytokine levels (left: adiponectin, middle: TNFα, right: leptin) in LacZ mice and UCP1 mice after a 10 hr fast on day 3 after adenoviral administration.

B) Relative amounts of leptin mRNA in adipose tissues.

C) Total food intakes on days 2 and 3 after adenoviral administration.

D) Relative amounts of neuropeptide Y (left) and proopiomelanocortin (right) mRNA were measured by quantitative RT-PCR using total RNA obtained from the hypothalamus on day 2 after adenoviral administration. Data were corrected with β-actin as the standard (**B** and **D**).

E and F) Leptin-tolerance tests were performed on day 3 after adenoviral administration. Data were expressed as ratios to the food intakes of vehicle-treated mice (**E**). Mice were weighed at 12 hr after each daily injection of leptin or vehicle (**F**).

G–K) LacZ (black bars) or UCP1 (white bars) adenovirus was injected into Epi of db/db mice.

G) Total food intakes on days 2 and 3 after adenoviral administration are presented.

H–K) Blood leptin (**H**), glucose (**I**), and insulin (**J**) levels and serum lipid parameters ([**K**]; left: triglyceride, right: free fatty acids) of db/db mice were measured after a 10 hr fast. Data are presented as means ± SD (n = 8 per group). *p < 0.05; **p < 0.01 by unpaired t test.

leptin mRNA expression was markedly decreased in intra-abdominal fat tissues (Figure 2B). Thus, the effects of UCP1 expression in Epi are also exerted in fat tissues other than those injected with the adenovirus. Food intake was significantly suppressed (Figure 2C), indicating that hypothalamic leptin sensitivity was markedly improved despite the lack of significant changes in body weights. Decreased leptin expression in several adipose tissues suggests efferent sympathetic nerve activation, which also supports leptin signal enhancement.

Administration of green fluorescent protein-adenovirus exerted minimal metabolic effects (Figures S1F–S1J). On day 7, when adenoviral UCP1 expression was markedly decreased (Figure S1B), blood glucose, insulin, and leptin levels did not differ between the UCP1 and LacZ mice (Figure S2). In addition, we confirmed the metabolic effects of UCP1 expression in Epi using three other obese models: AKR mice on high-fat chow and KK mice and KK-Ay mice on normal chow. In these three models, similar metabolic impacts were observed with UCP1 adenovirus administration into Epi (Figure S3). Thus, UCP1 expression in Epi exerts acute, beneficial metabolic effects in both diet-induced and genetically obese models.

Increased leptin signals in the hypothalamus induced by UCP1 expression in Epi were further confirmed by changed levels of hypothalamic neuropeptide expression in UCP1 mice on day 3 after adenoviral administration. Real-time RT-PCR revealed adipose UCP1 expression to significantly decrease expression of neuropeptide Y, an orexigenic neuropeptide, while tending to increase that of proopiomelanocortin, a precursor of an anorexigenic neuropeptide, in the hypothalamus (Figure 2D).

To directly test whether leptin sensitivity was improved, we performed leptin-tolerance tests. When leptin was injected intraperitoneally into fasting mice on day 3, leptin-induced food-intake inhibition was far more profound in UCP1 mice than in LacZ mice (Figure 2E). In addition, when leptin was given daily, body weights were significantly decreased (Figure 2F). Thus,

even very limited UCP1 expression in Epi exerts a remote therapeutic effect on hypothalamic leptin resistance, which had already developed in response to preloading with high-fat chow. Transgenic overexpression of UCP1 (Kopecky et al., 1995) and rather minor induction of UCP1 in white adipose tissue (Cederberg et al., 2001; Leonardsson et al., 2004; Tsukiyama-Kohara et al., 2001; Um et al., 2004) result in resistance to high-fat-diet-induced obesity but do not reportedly cause hypophagia. In this study, however, we expressed UCP1 after the development of obesity and leptin resistance and were thus able to observe acute, beneficial effects, i.e., improved leptin sensitivity, which would be difficult to detect using congenitally UCP1-overexpressing mice.

Increased leptin sensitivity is likely to be involved in the phenotype of UCP1 mice. If this is the case, at least some of the phenotypic features of UCP1 mice would presumably be absent in mice lacking the hypothalamic leptin signal. To test this, UCP1 or LacZ adenovirus was injected into Epi of db/db mice, leptin-receptor Ob-Rb mutants. Food intake (Figure 2G) and serum leptin (Figure 2H) did not differ between LacZ-expressing and UCP1-expressing db/db mice. These findings confirm that the effect of UCP1 expression in Epi on food intake is leptin-signal dependent. On the other hand, UCP1 expression in Epi of db/db mice caused small but significant decreases in blood glucose (Figure 2I), insulin (Figure 2J), and triglyceride (Figure 2K) levels, as well as tending to decrease serum free-fatty-acid levels (Figure 2K). These findings demonstrate that UCP1 expression in Epi improves insulin sensitivity, in part, independently of leptin signaling.

To eliminate the secondary effects of reduced food intake, pair-feeding experiments were performed using C57BL/6 wild-type mice (Figure S4). Pair feeding did not significantly alter the body weights of LacZ mice. Fasting blood glucose did not differ between UCP1 mice and pair-fed LacZ mice, but after glucose loading, blood glucose levels were significantly lower in UCP1 mice. In addition, serum insulin and leptin levels were significantly lower in UCP1 mice than in pair-fed LacZ mice. Taken together with the results obtained using db/db mice, the improved insulin sensitivity induced by UCP1 expression in Epi appears not to be mediated solely by decreased food intake.

The same amounts of recombinant adenovirus encoding UCP1 were directly injected into subcutaneous fat tissues in the flank of C57BL/6 mice with dietary obesity and diabetes. UCP1 expression levels were similar to those obtained by injection into Epi (data not shown). Food intake was significantly decreased by UCP1 expression, as compared with LacZ expression, in subcutaneous fat (Figure 3A), but the effects were much smaller than those produced by UCP1 expression in Epi (Figure 2C). Furthermore, there were no statistically significant decreases in blood glucose (Figure 3B), insulin (Figure 3C), or leptin (Figure 3D) levels. Thus, exogenous UCP1 expression in subcutaneous fat was far less effective in improving insulin and leptin resistance than that in intra-abdominal fat tissue. These findings suggest the anatomical location of the manipulated adipose tissue to be involved in the observed therapeutic effects, which would appear to be important for understanding the metabolic differences between visceral fat-dominant and subcutaneous fat-dominant obesity.

How does the signal (or signals) from intra-abdominal fat tissue exert these remote effects? The importance of anatomical fat-tissue location suggests the involvement of neuronal signaling. The afferent activity from Epi is reportedly transmitted through the nerve bundle, which runs alongside blood vessels supplying Epi, in rats (Niijima, 1998). To study the possible involvement of neuronal signals from Epi, we dissected this nerve bundle in mice with dietary obesity and diabetes. Ten days after bilateral nerve-bundle dissection, adenoviruses were injected into Epi. No significant differences in body weights or Epi weights were observed between sham-operated and nerve-dissected mice (data not shown). While UCP1 adenoviral administration significantly decreased food intake in sham-operated mice, nerve dissection blunted this decrease in food intake such that it was no longer statistically significant (Figure 3E). Similarly, nerve dissection blunted a decrease in hypothalamic NPY mRNA expression, rendering it statistically insignificant (NPY; LacZ versus UCP1: 12.06 ± 6.16 versus 6.39 ± 3.10; $p = 0.15$). These findings suggest that neuronal signals from intra-abdominal fat tissue are involved in food-intake regulation. In contrast, in nerve-dissected mice, blood glucose (Figure 3F) as well as serum insulin (Figure 3G) and leptin (Figure 3H) levels were significantly suppressed in a fashion similar to in sham-operated mice. Thus, improved insulin resistance is largely independent of this neuronal pathway.

To confirm that afferent-nerve signals are involved in UCP1-expression-mediated suppression of food intake, we next examined the effects of functional deafferentation by administering capsaicin (Fu et al., 2003), a selective neurotoxin for unmyelinated C fibers. In LacZ mice, food intake was not altered by capsaicin treatment 10 days prior to adenoviral administration. In contrast, capsaicin pretreatment significantly reversed the food-intake suppression induced by UCP1 expression in Epi (Figure 3I). The inhibitory effect of capsaicin pretreatment was very similar to that of local-nerve dissection (Figure 3E). Taken together, these observations suggest that afferent-nerve signals from Epi are involved in food-intake regulation. To elucidate the molecular mechanism whereby UCP1 expression in Epi modulates neuronal activity, we searched for genes upregulated by adipose UCP1 expression. Using the DNA microarray technique, gene expressions were examined in LacZ- and UCP1-adenovirus-treated Epi (Table S1) and in 3T3-L1 adipocytes (Table S2). With the exception of UCP1, however, there was no overlap in genes showing significantly increased expression. Although further expression profiling including proteomic approaches might elucidate the underlying mechanisms, the apparent lack of genes showing increased expression raises the possibility that the activation of afferent nerves does not involve gene-expression alterations. For instance, UCP1 generates heat, and a capsaicin receptor, TRPV1, is activated by a slightly above normal body temperature (Caterina et al., 1997). Capsaicin treatment affected UCP1-induced food-intake suppression (Figure 3I), raising the possibility that UCP1 expression activates capsaicin-sensitive nerves via TRPV1 activation. Another possibility is involvement of reactive oxygen species, which are affected by mitochondrial uncoupling (Bernal-Mizrachi et al., 2005; Jezek et al., 2004) and reportedly regulate capsaicin-sensitive afferent fibers (Ruan et al., 2005). Further studies are required to examine these hypotheses.

In this study, very limited UCP1 expression in Epi markedly improved insulin and leptin resistance, thereby improving glucose tolerance and decreasing food intake. UCP1 mice were more insulin sensitive than pair-fed LacZ mice. In addition, in db/db mice, despite no food-intake suppression, blood glucose

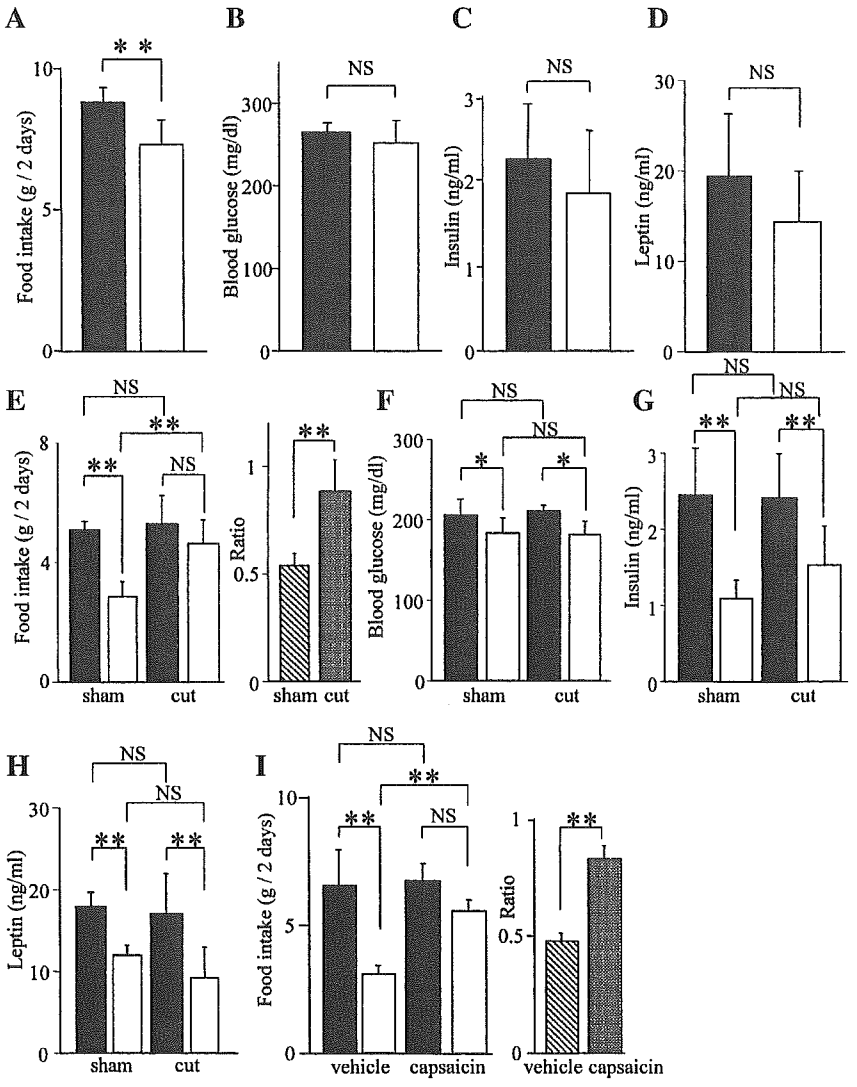

Figure 3. Neuronal signals are likely to be involved in food-intake regulation

A–D) LacZ (black bars) or UCP1 (white bars) adenovirus was injected into subcutaneous fat, and metabolic markers were measured. Total food intakes on days 2 and 3 after adenoviral administration are presented. Blood glucose (**B**), insulin (**C**), and leptin (**D**) levels were determined after a 10 hr fast on day 3 after adenoviral administration. **p < 0.01 by unpaired t test.

E–H) Mice were subjected to local-nerve dissection 10 days prior to adenoviral injection into Epi. Total food intakes of sham-operated (sham) and nerve-dissected (cut) mice (**E**) on days 2 and 3 are presented graphically. Blood glucose (**F**), serum insulin (**G**), and leptin (**H**) levels were determined on day 3.

I) Mice were treated with capsaicin or vehicle 10 days prior to adenoviral injection into Epi. Total food intakes on days 2 and 3 after administration of LacZ (black bars) or UCP1 (white bars) adenovirus are presented. In (**E**) and (**I**), the food intakes of UCP1 mice are expressed in the right graph as ratios to those of LacZ mice. **p < 0.01 assessed by one-factor ANOVA. Data are presented as means ± SD.

and insulin levels were modestly but significantly decreased by UCP1 expression in Epi. Thus, the mechanism underlying improved insulin sensitivity with UCP1 expression in Epi is, in part, independent of leptin signaling and food-intake suppression (Figure 4). Dissection of the nerve bundle from Epi did not alter the decreases in blood glucose and insulin levels. Taken together with the findings that UCP1 expression in subcutaneous fat did not significantly decrease blood glucose or insulin levels, our observations indicate that nonneuronal signals including humoral factors from intra-abdominal adipose tissue possibly participate in systemic improvement of insulin resistance. Since UCP1 expression was observed in a very limited population of adipocytes in Epi, suppression of insulin-resistant adipocytokine secretion is unlikely to explain the beneficial effects. Serum adiponectin levels were not altered, suggesting involvement of other unknown insulin-sensitizing factor (or factors).

On the other hand, decreased food intake is likely to be, at least partially, mediated by afferent-nerve signals from Epi (Figure 4). Afferent-nerve signals from Epi to the central nervous system reportedly result in a reflex from epididymal fat to white adipose tissues via efferent sympathetic-nerve activation (Niijima, 1998; Tanida et al., 2000). In addition, vagal afferent

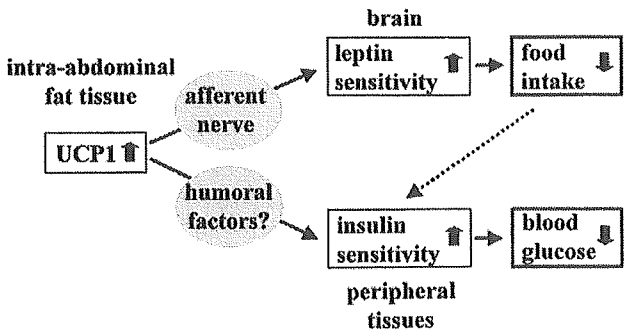

Figure 4. The proposed mechanism whereby UCP1 expression in Epi decreases food intake and improves glucose tolerance

neuronal signals from intra-abdominal tissues, including the gut (Fu et al., 2003; Smith et al., 1981) and the liver (Friedman, 1998; Scharrer, 1999), are known to play a part in regulating food intake. We also reported that UCP1 gene administration into the liver modulates food intake (Ishigaki et al., 2005). Herein we report that intra-abdominal fat tissue is likely to convey metabolic signals to the brain via a neuronal pathway, in addition to via the circulation, resulting in modulation of food intake. Although the precise molecular mechanism remains to be elucidated, this neuronal pathway might play a role in development of the metabolic syndrome, making it a potentially novel therapeutic target.

Experimental procedures

Preparation of recombinant adenovirus

Recombinant adenovirus containing murine UCP1 cDNA (Ishigaki et al., 2005) was constructed as described previously (Katagiri et al., 1996). Recombinant adenoviruses bearing the bacterial β-galactosidase gene (*Adex1CAlacZ*) and green fluorescent protein (AdCMV-GFP) were used as controls.

Animals and in vivo adenovirus injection into fat pad

Animal studies were conducted in accordance with the institutional guidelines for animal experiments at Tohoku University. Male C57BL/6N and AKR/N mice were housed individually, and high-fat-chow feeding (32% safflower oil, 33.1% casein, 17.6% sucrose, and 5.6% cellulose) (Ishigaki et al., 2005) was initiated at 5 weeks of age. After 4 weeks of high-fat-chow loading, body-weight-matched mice were anesthetized prior to dissection of the skin and body wall. The adenoviral preparation (1×10^8 plaque-forming units in a volume of 20 μl) was injected at two points each on each side of the epididymal fat pad or subcutaneous fat tissues in the flank, i.e., a total of four points. KK mice and KK-Ay mice maintained on a standard diet (65% carbohydrate, 4% fat, 24% protein) were similarly administered adenoviruses at 9 weeks and 5 weeks of age, respectively.

Immunoblotting

Tissue protein extracts (250 μg total protein) were boiled in Laemmli buffer containing 10 mM dithiothreitol, subjected to SDS-polyacrylamide gel electrophoresis, and transferred onto nitrocellulose filters. The filters were incubated with anti-UCP1 antibody (Santa Cruz Biotechnology, Santa Cruz, California) and then with anti-goat immunoglobulin G coupled to horseradish peroxidase. The immunoblots were visualized with an enhanced chemiluminescence detection kit (Amersham, Buckinghamshire, UK). The intensities of bands were quantified with the NIH Image 1.62 program.

Histological analysis

Mouse epididymal fat and BAT were immunostained as previously reported (Ishigaki et al., 2005). Mature white adipocytes were identified by their characteristic unilocular appearance. Diameters of 100 or more white adipocytes per mouse in each group were traced manually and analyzed.

Oxygen consumption

Oxygen consumption was measured as previously reported (Ishigaki et al., 2005).

Pair-feeding experiments

Pair-feeding experiments were performed as previously described (Ishigaki et al., 2005).

Blood analysis

Blood glucose and serum insulin, leptin, adiponectin, TNFα, total cholesterol, triglyceride, and free-fatty-acid levels were determined as previously described (Ishigaki et al., 2005).

Measurement of quantitative RT-PCR-based gene expression

The skull was reflected from the brain and the hypothalamus was isolated by snap freezing in liquid nitrogen as previously reported (Bjorbaek et al., 1998). Total RNA was isolated from mouse hypothalamus, fat tissues, or 3T3-L1 adipocytes with ISOGEN (Wako Pure Chemical Co., Osaka, Japan), and cDNA synthesized from total RNA was evaluated with a real-time PCR quantitative system (Light Cycler Quick System 350S; Roche Diagnostics GmbH, Mannheim, Germany).The relative amount of mRNA was calculated with β-actin mRNA as the invariant control. The primers used are shown in Table S3.

Glucose-, insulin-, and leptin-tolerance tests

Glucose-tolerance tests were performed on fasted (10 hr, daytime) mice. Mice were given glucose (2 g/kg of body weight) intraperitoneally, followed by measurement of blood glucose levels. Insulin-tolerance tests were performed on ad libitum-fed mice. Mice were intraperitoneally injected with human regular insulin (0.75 U/kg of body weight; Eli Lilly Co., Kobe, Japan).

Leptin-tolerance tests were carried out as described in a previous report (Igel et al., 1997), with slight modification. Fasted (12 hr) mice were injected with mouse leptin (7.2 mg/kg of body weight; R&D Systems, Inc.) intraperitoneally, and food intakes were monitored for 12 hr after the injection. To examine effects on body-weight change, these two groups of mice were given leptin daily starting on the day of adenoviral administration. Each mouse was then weighed.

Capsaicin treatments

Capsaicin treatment was performed as described in a previous report (Fu et al., 2003), with minor modification. Mice were anesthetized prior to subcutaneous injection of capsaicin solution (50 mg/kg, 12.5 mg/ml dissolved in vehicle). The control group received vehicle treatment (10% Tween 80, 10% ethanol, and 80% saline) under identical administration conditions. Adenoviral administration into Epi was carried out 10 days later.

Local-nerve dissection

The small nerve bundle which runs along side blood vessels supplying Epi was dissected as previously reported (Niijima, 1998). Ten days after bilateral dissection of this nerve bundle, adenoviruses were injected into epididymal fat pad.

Measurement of ATP

Fully differentiated 3T3-L1 adipocytes were infected with recombinant adenoviruses as previously described (Katagiri et al., 1996). Intracellular ATP levels were measured using an ATP determination kit (TOYO B-Net, Tokyo, Japan).

Microarray experiments

Total RNA from epididymal fat or 3T3-L1 adipocytes was used to synthesize cRNA, which was then hybridized to an HG-U133A oligonucleotide array (Affymetrix, Santa Clara, California) according to standard protocols, as described previously (Hippo et al., 2002).

Statistical analysis

All data were expressed as means ± SD. The statistical significance of differences was assessed by the unpaired t test and one-factor ANOVA.

Supplemental data

Supplemental Data include four figures and three tables and can be found with this article online at http://www.cellmetabolism.org/cgi/content/full/3/3/223/DC1/.

Acknowledgments

We appreciate Drs. L.P. Kozak (Pennington Biomedical Research Center) and H. Mizuguchi (National Institute of Biomedical Innovation) for the generous gifts of UCP1 cDNA and GFP-adenovirus, respectively. We thank Ms. H. Meguro (Tokyo University) for technical support. This work was supported by a Grant-in-Aid for Scientific Research (B2, 15390282) and a Grant-in-Aid for Exploratory Research (15659214) to H.K. from the Ministry of Education, Science, Sports and Culture of Japan and a Grant-in-Aid for Scientific Research (H16-genome-003) to Y.O. from the Ministry of Health, Labor and Welfare of Japan. This work was also supported by the 21st Century COE Programs "CRESCENDO" (H.K.) and "the Center for Innovative Therapeutic Development for Common Diseases" (Y.O.) of the Ministry of Education, Science, Sports and Culture.

Received: June 22, 2005
Revised: October 12, 2005
Accepted: February 1, 2006
Published: March 7, 2006

References

Bernal-Mizrachi, C., Gates, A.C., Weng, S., Imamura, T., Knutsen, R.H., DeSantis, P., Coleman, T., Townsend, R.R., Muglia, L.J., and Semenkovich, C.F. (2005). Vascular respiratory uncoupling increases blood pressure and atherosclerosis. Nature *435*, 502–506.

Bjorbaek, C., Elmquist, J.K., Frantz, J.D., Shoelson, S.E., and Flier, J.S. (1998). Identification of SOCS-3 as a potential mediator of central leptin resistance. Mol. Cell *1*, 619–625.

Bjorntorp, P. (1992). Abdominal fat distribution and disease: an overview of epidemiological data. Ann. Med. *24*, 15–18.

Caterina, M.J., Schumacher, M.A., Tominaga, M., Rosen, T.A., Levine, J.D., and Julius, D. (1997). The capsaicin receptor: a heat-activated ion channel in the pain pathway. Nature *389*, 816–824.

Cederberg, A., Gronning, L.M., Ahren, B., Tasken, K., Carlsson, P., and Enerback, S. (2001). FOXC2 is a winged helix gene that counteracts obesity, hypertriglyceridemia, and diet-induced insulin resistance. Cell *106*, 563–573.

Considine, R.V., Sinha, M.K., Heiman, M.L., Kriauciunas, A., Stephens, T.W., Nyce, M.R., Ohannesian, J.P., Marco, C.C., McKee, L.J., Bauer, T.L., et al. (1996). Serum immunoreactive-leptin concentrations in normal-weight and obese humans. N. Engl. J. Med. *334*, 292–295.

Flier, J.S. (2004). Obesity wars: molecular progress confronts an expanding epidemic. Cell *116*, 337–350.

Friedman, J.M. (2003). A war on obesity, not the obese. Science *299*, 856–858.

Friedman, J.M., and Halaas, J.L. (1998). Leptin and the regulation of body weight in mammals. Nature *395*, 763–770.

Friedman, M.I. (1998). Fuel partitioning and food intake. Am. J. Clin. Nutr. *67*, 513S–518S.

Fu, J., Gaetani, S., Oveisi, F., Lo Verme, J., Serrano, A., Rodriguez De Fonseca, F., Rosengarth, A., Luecke, H., Di Giacomo, B., Tarzia, G., and Piomelli, D. (2003). Oleylethanolamide regulates feeding and body weight through activation of the nuclear receptor PPAR-alpha. Nature *425*, 90–93.

Heymsfield, S.B., Greenberg, A.S., Fujioka, K., Dixon, R.M., Kushner, R., Hunt, T., Lubina, J.A., Patane, J., Self, B., Hunt, P., and McCamish, M. (1999). Recombinant leptin for weight loss in obese and lean adults: a randomized, controlled, dose-escalation trial. JAMA *282*, 1568–1575.

Hippo, Y., Taniguchi, H., Tsutsumi, S., Machida, N., Chong, J.M., Fukayama, M., Kodama, T., and Aburatani, H. (2002). Global gene expression analysis of gastric cancer by oligonucleotide microarrays. Cancer Res. *62*, 233–240.

Igel, M., Becker, W., Herberg, L., and Joost, H.G. (1997). Hyperleptinemia, leptin resistance, and polymorphic leptin receptor in the New Zealand obese mouse. Endocrinology *138*, 4234–4239.

Ishigaki, Y., Katagiri, H., Yamada, T., Ogihara, T., Imai, J., Uno, K., Hasegawa, Y., Gao, J., Ishihara, H., Shimosegawa, T., et al. (2005). Dissipating excess energy stored in the liver is a potential treatment strategy for diabetes associated with obesity. Diabetes *54*, 322–332.

Jezek, P., Zackova, M., Ruzicka, M., Skobisova, E., and Jaburek, M. (2004). Mitochondrial uncoupling proteins—facts and fantasies. Physiol. Res. *53* Suppl. 1, S199–S211.

Katagiri, H., Asano, T., Ishihara, H., Inukai, K., Shibasaki, Y., Kikuchi, M., Yazaki, Y., and Oka, Y. (1996). Overexpression of catalytic subunit p110alpha of phosphatidylinositol 3-kinase increases glucose transport activity with translocation of glucose transporters in 3T3-L1 adipocytes. J. Biol. Chem. *271*, 16987–16990.

Klingenberg, M., and Huang, S.G. (1999). Structure and function of the uncoupling protein from brown adipose tissue. Biochim. Biophys. Acta *1415*, 271–296.

Kopecky, J., Clarke, G., Enerback, S., Spiegelman, B., and Kozak, L.P. (1995). Expression of the mitochondrial uncoupling protein gene from the aP2 gene promoter prevents genetic obesity. J. Clin. Invest. *96*, 2914–2923.

Leonardsson, G., Steel, J.H., Christian, M., Pocock, V., Milligan, S., Bell, J., So, P.W., Medina-Gomez, G., Vidal-Puig, A., White, R., and Parker, M.G. (2004). Nuclear receptor corepressor RIP140 regulates fat accumulation. Proc. Natl. Acad. Sci. USA *101*, 8437–8442.

Matsuzawa, Y., Shimomura, I., Nakamura, T., Keno, Y., and Tokunaga, K. (1995). Pathophysiology and pathogenesis of visceral fat obesity. Ann. N Y Acad. Sci. *748*, 399–406.

Niijima, A. (1998). Afferent signals from leptin sensors in the white adipose tissue of the epididymis, and their reflex effect in the rat. J. Auton. Nerv. Syst. *73*, 19–25.

Ruan, T., Lin, Y.S., Lin, K.S., and Kou, Y.R. (2005). Sensory transduction of pulmonary reactive oxygen species by capsaicin-sensitive vagal lung afferent fibres in rats. J. Physiol. *565*, 563–578.

Scharrer, E. (1999). Control of food intake by fatty acid oxidation and ketogenesis. Nutrition *15*, 704–714.

Smith, G.P., Jerome, C., Cushin, B.J., Eterno, R., and Simansky, K.J. (1981). Abdominal vagotomy blocks the satiety effect of cholecystokinin in the rat. Science *213*, 1036–1037.

Tanida, M., Iwashita, S., Ootsuka, Y., Terui, N., and Suzuki, M. (2000). Leptin injection into white adipose tissue elevates renal sympathetic nerve activity dose-dependently through the afferent nerves pathway in rats. Neurosci. Lett. *293*, 107–110.

Tsukiyama-Kohara, K., Poulin, F., Kohara, M., DeMaria, C.T., Cheng, A., Wu, Z., Gingras, A.C., Katsume, A., Elchebly, M., Spiegelman, B.M., et al. (2001). Adipose tissue reduction in mice lacking the translational inhibitor 4E-BP1. Nat. Med. *7*, 1128–1132.

Um, S.H., Frigerio, F., Watanabe, M., Picard, F., Joaquin, M., Sticker, M., Fumagalli, S., Allegrini, P.R., Kozma, S.C., Auwerx, J., and Thomas, G. (2004). Absence of S6K1 protects against age- and diet-induced obesity while enhancing insulin sensitivity. Nature *431*, 200–205.

Available online at www.sciencedirect.com
SCIENCE DIRECT
ELSEVIER
Biochemical and Biophysical Research Communications 339 (2006) 533–539
BBRC
www.elsevier.com/locate/ybbrc

Transcriptional activity of Pax3 is co-activated by TAZ ☆

Masao Murakami [a,c,1], Junji Tominaga [a,b,1], Ryosuke Makita [b], Yasunobu Uchijima [b], Yukiko Kurihara [b], Osamu Nakagawa [c], Tomoichiro Asano [b], Hiroki Kurihara [b,*]

[a] *Department of Integrative Cell Biology, Institute of Molecular Embryology and Genetics, Kumamoto University, 2-2-1 Honjo, Kumamoto, Kumamoto 860-0811, Japan*
[b] *Department of Physiological Chemistry and Metabolism, Graduate School of Medicine, The University of Tokyo, 7-3-1 Hongo, Bunkyo-ku, Tokyo 113-0033, Japan*
[c] *Division of Cardiology, Department of Internal Medicine, and Department of Molecular Biology, The University of Texas Southwestern Medical Center at Dallas, 6000 Harry Hines Blvd., Dallas, TX 75390-9148, USA*

Received 11 October 2005
Available online 15 November 2005

Abstract

Pax3 is a transcription factor which functions in embryonic development and human diseases. In a yeast two-hybrid screen with full-length Pax3 as bait, we isolated a clone encoding transcriptional co-activator with PDZ-binding motif (TAZ) from an E10.5 mouse embryo cDNA library. Co-immunoprecipitation and nuclear co-localization of TAZ with Pax3 suggest that their association is functionally relevant. In situ hybridization revealed *TAZ* and *Pax3* expression to partially overlap in the paraxial mesoderm, limb buds, and the neural tube. In C2C12 myoblast cells and NIH3T3 cells, TAZ enhanced the transcriptional activity of Pax3 on artificial and microphthalmia-associated transcription factor promoter-luciferase constructs, suggesting that TAZ can function as a co-activator of Pax3. Functional interaction between Pax3 and TAZ may provide a clue to clarifying the mechanism by which Pax3 serves as a transcriptional activator during embryogenesis.

Keywords: Pax3; TAZ; Co-activator; Transcription

Pax3 is a member of the Pax gene family, consisting of nine members defined by a highly conserved DNA binding domain known as the paired domain (PD), which shares sequence homology with *Paired*, a *Drosophila* segmentation gene [1–3]. Pax3 also possesses a homeodomain (HD), another conserved DNA binding motif, and acts as a transcription factor to regulate the expression of genes, such as c-*ret*, c-*met*, and *MITF* [4–6]. During embryogenesis, Pax3 is expressed in the dorsal neural tube, neural crest derivatives, and paraxial mesoderm-derived skeletal muscle progenitors [1–3]. *Splotch* mice, harboring spontaneous mutations in *Pax3*, demonstrate defects in neural tube closure, cardiovascular morphogenesis, pigmentation, and limb myogenesis [7–10]. In humans, Waardenburg syndrome type I and III, characterized by facial, hearing, pigmentation, and limb abnormalities, are caused by mutations in *PAX3* [11–13]. Furthermore, PAX3-FKHR, a fusion protein between the C-terminal transactivation domain of FKHR (FOXO1A) and the DNA binding domain of Pax3 resulting from a chromosome translocation t (2; 13), can cause alveolar rhabdomyosarcomas [14–16].

To date, several nuclear proteins, such as Daxx and pRb, have been shown to interact physically with Pax3 and inhibit Pax3 activity [17,18]. HIRA, a homolog of the yeast transcriptional corepressors Hir1p and Hir2p, and Mox2, an Antennapedia-like homeobox-containing protein, have also been reported to associate with Pax3,

☆ *Abbreviations:* TAZ, transcriptional co-activator with PDZ-binding motif; YAP, yes-associated protein; MITF, microphthalmia-associated transcription factor; GST, glutathione *S*-transferase.

* Corresponding author. Fax: +81 3 5684 4958.
E-mail address: kuri-tky@umin.ac.jp (H. Kurihara).

[1] These authors contributed equally to this work.

0006-291X/$ - see front matter © 2005 Elsevier Inc. All rights reserved.
doi:10.1016/j.bbrc.2005.10.214

but their effects on the transcriptional activity of Pax3 have yet to be determined [19,20]. To obtain further information about protein–protein interactions modulating the function of Pax3, we screened for proteins that bind to Pax3 using the yeast two-hybrid system. Herein we identified TAZ as a molecule that binds to Pax3. We showed TAZ and Pax3 to be co-expressed in the paraxial mesoderm, limb buds and the neural tube during embryogenesis, and to be co-localized in the nucleus. Furthermore, TAZ can stimulate the transcriptional activity of Pax3 in cultured cells. These findings suggest that TAZ serves as a transcriptional co-activator for Pax3 and that this association may contribute to embryonic development.

Materials and methods

Plasmid constructions. Mouse Pax3 and TAZ cDNAs were amplified by PCR from E10.5 mouse embryo cDNA. Pax3 cDNA was subcloned into pDBLeu vector (Life Technologies) to generate pDBLeu-Pax3 as bait for the yeast two-hybrid screening. Pax3 or TAZ cDNAs were cloned into the 3′ cloning sites of the epitope-tagged expression vectors pCEFL-AU5 [21], pCEFL-HA [21], and pGEX (Amersham Pharmacia Biotech). Point mutants of Pax3 were constructed using a Quick Change XL Site-Directed Mutagenesis kit (Stratagene) and were inserted into the expression vectors. For $p(PRS\text{-}1/\text{-}4)_3$-Luc, a reporter construct for the luciferase assay, two oligonucleotides complementary to each other, 5′-ATTA CGTTCCAGATTACGTTCCAGATTACGTTCC-3′ and 5′-GGAACG TAATCTGGAACGTAATCTGGAACGTAAT-3′ were annealed and ligated to the minimal promoter in pLuc-MCS. For pMITF-Luc, the 5′-flanking sequence of the mouse *Mitf* gene (−387 to +99) was cloned by PCR from mouse genomic DNA and inserted into pGL3-Basic (Promega).

Yeast two-hybrid screening. Yeast two-hybrid screening was carried out according to the manufacturer's protocol for the ProQuest two-hybrid system (Life Technologies).

Cell culture and transfection. Cell culture conditions of 293T, NIH3T3, and C2C12 cells are described previously [22]. Transfection was performed using Lipofectamine Plus reagent (Life Technologies).

Pull-down assay, co-immunoprecipitation, and Western blotting. Preparation of GST-fusion proteins and cell lysates is described previously [22,23]. GST, GST-TAZ, and derivatives bound to glutathione beads were incubated at 4 °C for more than 2 h with cell lysates prepared from 293T cells expressing AU5-Pax3 proteins. After extensive washing, bound proteins were detected by Western blotting. For co-immunoprecipitation (co-IP) experiment, cell lysates of 293T cells expressing exogenous proteins were treated with anti-AU5 antibody and the immunoprecipitants were subjected to 10% SDS–PAGE. Proteins binding to AU5-Pax3 were detected by Western blotting using anti-HA antibody (Covance), as described previously [22,23].

In situ hybridization. Antisense and sense RNA probes were prepared from cDNA fragments by T3 or T7 RNA polymerase using a DIG RNA labeling kit (Roche). The procedure of in situ hybridization was described previously [24].

Preparation of anti-TAZ antibody. Polyclonal antibody against mouse TAZ was generated by injecting a rabbit with GST-TAZ. The bleeds were affinity-purified using Affi-Gel 10 gel (Bio-Rad) coupled with TAZ.

Immunocytochemistry. Cells were fixed with 4% paraformaldehyde in PBS, permeabilized with 0.2% Triton X-100 in PBS and washed with PBS at room temperature. After blocking with 5% skim milk in PBS, cells were incubated with the rabbit anti-TAZ antibody and mouse monoclonal anti-AU5 antibody. Then, cells were stained with secondary antibodies (FITC-conjugated donkey anti-rabbit IgG or rhodamine-conjugated goat anti-mouse IgG (Jackson Immunoresearch)) and viewed using a confocal microscope (Nikon D-ECLIPSE C1).

Luciferase assay. AU5- or HA-tagged expression constructs, reporter constructs, and pRL-SV40 (Promega) were co-transfected into C2C12 or NIH3T3 cells. Forty-eight hours after transfection, luciferase units in the cell lysates were determined with a luminometer. Transfection efficiency was normalized on the basis of *Renilla* luciferase activity.

Results

Identification of TAZ as a Pax3-binding protein

Using full-length Pax3 as bait, we screened about 2 million clones of the mouse E10.5 cDNA library for novel interacting partners. Thirty-four positive clones were obtained in the first screening, and the second screening with higher stringency revealed 6 clones to be candidates for Pax3-binding molecules. One was identified as encoding 359 amino acids (37–395) of TAZ, a transcriptional co-activator with PDZ-binding motif.

To demonstrate that Pax3 can physically interact with TAZ, we cloned full length TAZ and performed GST pull-down assay. As shown in Fig. 1A, Pax3 specifically associated with GST-TAZ but not with GST alone. To examine whether Pax3 can associate with TAZ in mammalian cells, we co-expressed AU5-Pax3 and HA-TAZ in 293T cells and performed co-IP experiments. HA-TAZ was coimmunoprecipitated only in the presence of Pax3 (Fig. 1B). These results indicate that Pax3 specifically interacts with TAZ both in vitro and in vivo.

Co-expression of TAZ and Pax3 in paraxial mesoderm, limb buds, and neural tube

Next, we investigated whether *TAZ* and *Pax3* genes are co-expressed in mouse embryonic tissues. In E9.5 embryos,

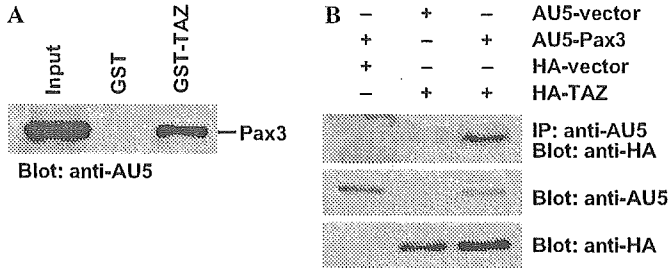

Fig. 1. Physical association between TAZ and Pax3. (A) Pull-down assay was performed using GST-TAZ, and AU5-Pax3 expressed in 293T cells. Interaction was detected by Western blotting using anti-AU5 antibody. (B) Co-IP experiment was performed using HA-TAZ and AU5-Pax3 expressed in 293T cells (upper). Expression of each protein was analyzed by Western blotting (lower).

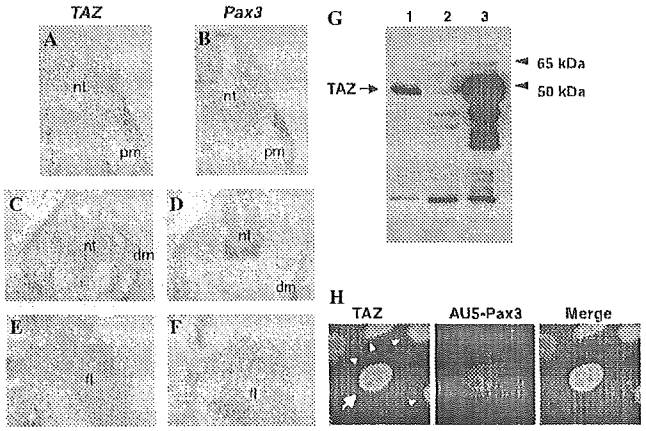

Fig. 2. Embryonic expression of TAZ and subcellular localization of TAZ in cultured cells. In situ hybridization with probes for *TAZ* (A,C,E) and *Pax3* (B,D,F) was performed on transverse sections of E9.5 (A,B) and E10.5 (C–F) mouse embryos. (A,B) Adjacent sections of an E9.5 embryo at the post-otic level. (C-F) Adjacent sections of an E10.5 embryo at the forelimb level. dm, dermomyotome; fl, forelimb; nt, neural tube; pm, paraxial mesoderm. (G) Western blot of endogenous and overexpressed TAZ: NIH3T3 (lane 1), 293T (lane 2), and AU5-TAZ-transfected 293T cells (lane 3). (H) Immunocytochemistry of NIH3T3 cells transfected with AU5-Pax3. Arrow and arrowheads indicates a Pax3-transfected cell and untransfected cells, respectively.

TAZ expression was detected in the paraxial mesoderm (Fig. 2A), where it partially overlapped with *Pax3* expression in dermomyotomes (Fig. 2B and [25,26]). In E10.5 embryos, *TAZ* expression was distributed in the somitic mesoderm and limb bud mesenchyme (Figs. 2C and E). At the same stage, *Pax3* was expressed in dermomyotomes and migrating muscle progenitors in limb buds (Figs. 2D and F and [25,26]). Thus, *TAZ* was co-expressed with *Pax3* in the skeletal muscle cell lineage, but appeared to be more diffuse than *Pax3* expression, suggesting *TAZ* to be widely expressed beyond the muscle cell lineage within the mesoderm.

TAZ was also expressed in the ventral and medial part of the neural tube at E10.5 (Fig. 2C). In contrast, *Pax3* was expressed in the dorsal half of the neural tube (Fig. 2D). Comparison of the expression domains of both genes indicates that *TAZ* and *Pax3* are co-expressed in the intermediate region between the dorsoventral halves (Figs. 2C and D).

Nuclear localization of TAZ in cultured cells

Next, we generated a rabbit polyclonal antibody against mouse TAZ and analyzed endogenous TAZ protein. Western blot analysis of lysates from NIH3T3 cells revealed this antibody to recognize a single band with a molecular mass of approximately 50 kDa (Fig. 2G, lane 1), which corresponded to the most intense band in 293T cells transfected with TAZ (Fig. 2G, lane 3).

We analyzed subcellular localization of TAZ and Pax3 in NIH3T3 cells. Endogenous TAZ immunoreactivity was detected predominantly in the nucleus, where exogenous Pax3 was also localized (Fig. 2H). TAZ was localized in the cytoplasm as well, but to a lesser extent (Fig. 2H). This result indicates that TAZ may act as a nuclear protein and interact with Pax3 in the nucleus.

TAZ acts as a transcriptional co-activator for Pax3

It is reported that TAZ can function as a co-activator of transcription factors [27–30]. To test whether TAZ can co-activate Pax3-dependent transcription, we performed a luciferase assay using the reporter plasmid in which three copies of the Pax3 binding element for both the HD and the PD (ATTA and GTTCC, respectively) were placed upstream from the luciferase gene ($p(PRS\text{-}1/\text{-}4)_3$-Luc) [9]. In C2C12 cells, Pax3 produced a 6-fold increase in luciferase activity as compared with the control (Fig. 3A). Co-expression of TAZ further augmented Pax3-dependent transcription in a dose-dependent manner (Fig. 3A). TAZ alone increased the basal transcription level by ~3.5-fold (Fig. 3A), possibly due to the presence of Pax3 or related transcription factors in C2C12 cells. We then examined the effect of TAZ on basal and Pax3-activated transcription in NIH3T3 cells, in which TAZ was expressed but Pax3 was not. Pax3 enhanced transcriptional activity by ~5.8-fold, and co-transfection of TAZ with Pax3 resulted in a ~11-fold increase in transcriptional activity over basal levels (Fig. 3B). However, transfection of TAZ alone did not enhance the basal activity at all (Fig. 3B).

To further confirm the co-activation of Pax3 by TAZ, we used pMITF-Luc, a reporter plasmid containing the promoter region of mouse *Mitf* gene. Pax3 or TAZ alone increased luciferase activity by ~7.7- and 2.2-fold as compared with the control, respectively (Fig. 3C). Co-transfection of TAZ with Pax3 resulted in a ~17-fold increase in luciferase activity (Fig. 3C). This result is consistent with the possibility that TAZ may act as a transcriptional co-activator of Pax3.

TAZ interacted with Pax3 via multiple domains

To identify the interaction domain, we made deletion mutants of Pax3 and TAZ as shown in Fig. 4 and examined their interactions by GST pull-down assay. Pax3 interacted with both TAZ (1–170) and TAZ (171–395) (Fig. 5A). TAZ also interacted with both Pax3-NM and Pax3-C (Fig. 5B). These results suggest that the interaction between Pax3 and TAZ may be through multiple domains. Pax3 has two L/PPXY motifs (PY-motifs) in its C-terminal region (Fig. 4). We have introduced point mutations into these sites to analyze the importance of the PY-motifs for interaction with TAZ. As shown in Fig. 5C, Pax3-C interacts with TAZ, but not Pax3C-AY, -YA, and -AA, suggesting that the interaction between C-terminal region of Pax3 and TAZ are through WW domain and PY-motif. To analyze which interactions are the strongest and the most specific, we made additional deletion mutants of TAZ and examined Pax3–TAZ interactions using more stringent

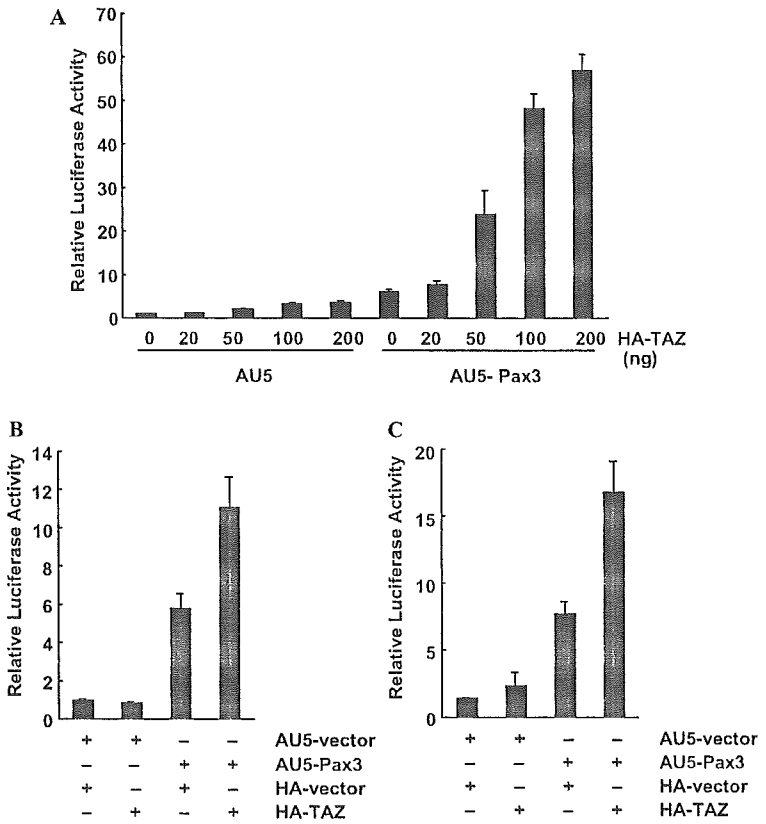

Fig. 3. TAZ coactivated Pax3-dependent transcription. (A) TAZ activated Pax3-dependent transcription in a dose-dependent manner. Different amounts of TAZ expression vector were cotransfected with 100 ng Pax3 vector and p(PRS-1/-4)$_3$-Luc into C2C12 cells, and luciferase assay was performed. (B) Luciferase assay was performed using NIH3T3 cells not expressing Pax3. (C) *MITF*-Luc was cotransfected together with expression vectors for TAZ (100 ng) and Pax3 (100 ng) into C2C12 cells, and luciferase assay was performed. Each value is expressed as the mean ± standard deviation of triplicate experiments.

conditions. As shown in Fig. 5D, a small fragment of TAZ (100–170) containing the WW domain physically interacted with both full length Pax3 and Pax3-C but not with Pax3-N or Pax3-M. To confirm the interaction of TAZ-WW domain is specific to PY-motif, we performed pull-down assay using Pax3 mutant lacking the PY-motifs. As shown in Fig. 5E, Pax3 but not Pax3-AA can bind to the TAZ-WW domain, indicating the interaction between TAZ-WW domain and Pax3 is PY-motif-specific. Under these conditions, TAZ (171–395) did not bind to Pax3 (Fig. 5D), suggesting a hypertonic condition might affect the interaction between the C-terminal region of TAZ and Pax3.

PY-motifs of Pax3 are not essential for the co-activation by TAZ

Next, we tested whether the association between the (L/P)PXY motif of Pax3 and the WW domain of TAZ was necessary for transcriptional co-activation by TAZ. For this purpose, we performed a reporter assay using point mutants of Pax3 lacking either or both of the two (L/P)PXY motifs. All the mutants tested, Pax3-AY, Pax3-YA, and Pax3-AA, activated transcription to the same degree as wild-type Pax3 (Fig. 6A). As shown in Fig. 6B, these Pax3 mutants without PY-motifs as well as wild-type Pax3 interacted with TAZ, suggesting that an interaction other than between the WW domain and PY-motifs is also important for the interaction with TAZ. Instead, Pax3-NM (1–285), a mutant lacking the C-terminal region, demonstrated neither transcriptional activation nor co-activation by TAZ (Fig. 6A). These results suggest that the C-terminal region of Pax3 may be essential for co-activation by TAZ, while the (L/P)PXY motifs in this region are not required and another interaction may be more important in vivo.

Discussion

In this study, we identified TAZ as a co-activator of Pax3. TAZ physically interacted with Pax3 and co-activated Pax3-dependent transcription on artificial and *Mitf* promoter-luciferase constructs.

Although Pax3 influences the expression of various genes during embryonic development, its mode of action

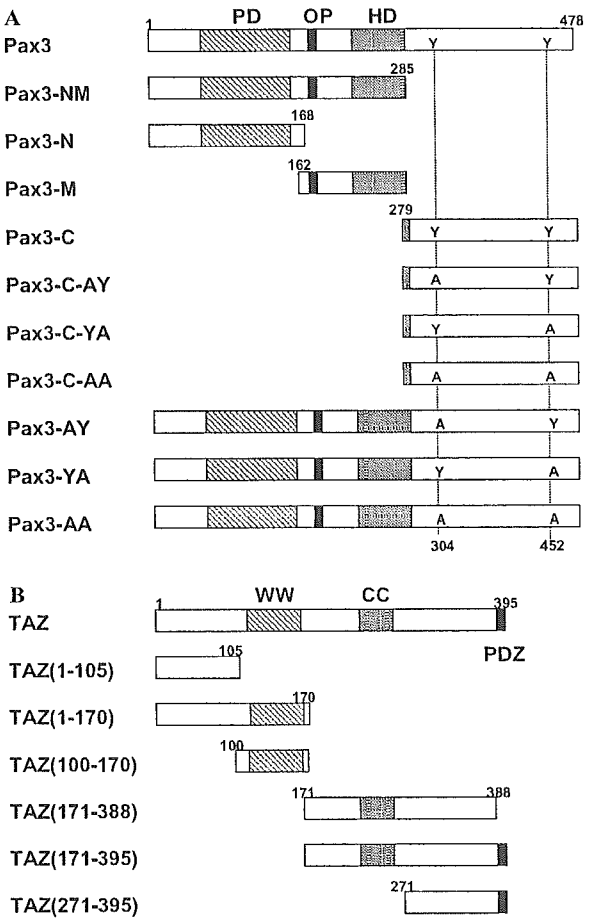

Fig. 4. The structures of mouse Pax3, TAZ, and mutated derivatives used in this study. (A) Pax3 and its mutants. Tyrosines at positions 304 and 452 are substituted with alanines in some mutants. PD, paired domain; OP, octapeptide domain; HD, homeodomain. (B) TAZ and its deletion mutants. WW, WW domain; CC, coiled-coil domain; PDZ, PDZ-binding motif.

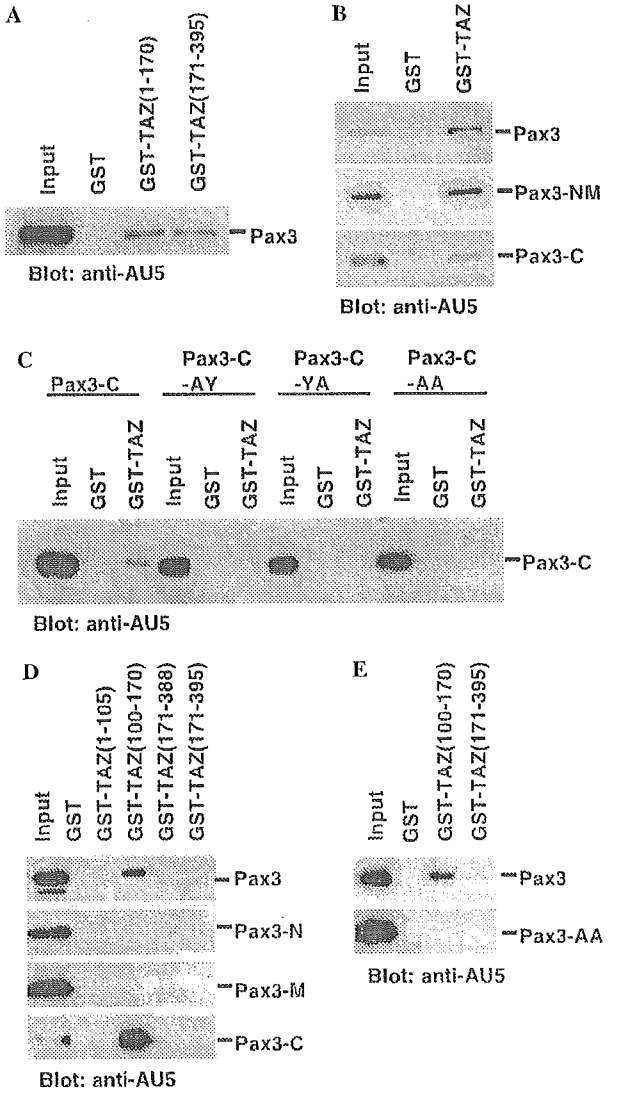

Fig. 5. Interaction domain analysis of TAZ and Pax3. (A–C) Pull-down assay was performed using GST-TAZ deletion mutants and AU5-Pax3 expressed in 293T cells. Bound proteins were detected by Western blotting using anti-AU5 antibody. (D,E) Pull-down assay using GST-TAZ deletion mutants and Pax3 mutants expressed in 293T cells in the presence of 0.5 M NaCl.

as a transcription factor remains poorly understood. Recently it has been reported that PAX3-FKHR, which is a potent gain-of-function mutation, rescues the defects of Pax3 mutant mice [14]. This suggests that Pax3 acts mainly as a transcriptional activator in vivo and indicates the importance of co-activators for Pax3 mediated transcription [14]. However, only co-repressors, such as Daxx and Rb [17,18], have been identified as Pax3 binding proteins to date. Our finding may be an important clue to elucidating the mechanisms that regulate Pax3 activity. Detailed analyses of TAZ may help to elucidate the activation mechanisms of Pax3.

TAZ was originally identified as a 14-3-3-binding molecule, and phosphorylation of TAZ affected the interaction with 14-3-3 and its subcellular localization [27]. This result suggests that the regulation of transcriptional activity by TAZ may be signal-responsive. TAZ shares homology with Yes-associated protein (YAP) especially in the WW domain, which is suggested to be responsible for binding to the (L/P)PXY motif present on interacting proteins. TAZ and YAP are expressed relatively ubiquitously [27] and might have the redundant function to co-activate the same transcription factors in some tissues.

Recently, it has been reported that TAZ acts as a transcriptional co-activator for Cbfa1, TTF1/Nkx2.1, and Runx2 [28–30]. Binding between the WW domain and (L/P)PXY motifs is assumed to mediate the interactions between TAZ and these transcriptional factors. Pax3 has two (L/P)PXY motifs in its C-terminal region. However, the present results indicate that TAZ can associate with Pax3 and co-activate its transcriptional activity without interaction between the WW domain and (L/P)PXY

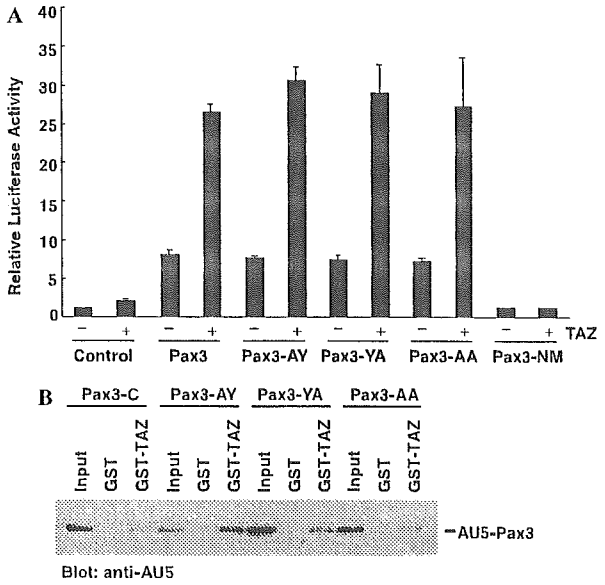

Fig. 6. (A) Expression vector for Pax3 mutants and TAZ were cotransfected with p(PRS-1/-4)$_3$-Luc into C2C12 cells, and luciferase assay was performed. Each value is expressed as the mean ± standard deviation of triplicate experiments. (B) Pull-down assay was performed using GST-TAZ and AU5-Pax3 mutants expressed in 293T cells. Bound proteins were detected by Western blotting using anti-AU5 antibody.

motifs. Deletion mutant analyses indicate either the N-terminal or C-terminal region of TAZ is sufficient for binding to Pax3 in pull-down assays, suggesting that TAZ binds to Pax3 via multiple domains. These results may suggest the possibility that TAZ can interact with transcription factors having no PY-motif and co-activate them. For Pax3 however, deletion of the C-terminal region abolished the basal and TAZ-dependent co-activation of transcription. This suggests that the C-terminal region of Pax3 is required for stimulation of gene expression, although the N-terminal region of Pax3 is sufficient for binding to TAZ in vitro. More detail analyses are necessary, and identification of other binding partners of TAZ may help us to elucidate the co-activation mechanisms of TAZ.

The present in situ hybridization analysis revealed *TAZ* and Pax3 expression to partially overlap in the paraxial mesoderm, limb buds, and the neural tube during mouse embryogenesis. This raises the possibility that TAZ and Pax3 may interact in a subset of myogenic and neurogenic cell lineages to regulate tissue-specific gene expression. However, the expression patterns of these two genes are markedly different overall, suggesting that the presence of TAZ may determine target gene specificity of Pax3. In non-myogenic cell lineages within the mesoderm, TAZ may associate with different transcription factors to control cell growth and differentiation.

In conclusion, TAZ has now emerged as a transcriptional co-activator for Pax3. This finding may provide an important clue to the mechanism by which the transcriptional activity of Pax3 is regulated and activates downstream genes to contribute to embryogenesis.

Acknowledgments

We thank Dr. E.M. Small for critical comments on this paper, and Ms. S. Okamura, Mr. Y. Kawamura, and Ms. K. Shin-Fukuhara for technical assistance. We are also grateful to members of the Gene Technology Center in Kumamoto University for their important contributions to the experiments. This work was supported by grants from the Japan Society for the Promotion of Science Research for the Future Program; Grants-in-Aid for scientific research from the Ministry of Education, Culture, Sports, Science and Technology, Japan; a Research Grant for Cardiovascular Diseases (14C-1) from the Ministry of Health, Labor and Welfare; a Research Grant from Uehara Memorial Foundation.

References

[1] M.D. Goulding, G. Chalepakis, U. Deutsch, J.R. Erselius, P. Gruss, Pax-3, a novel murine DNA binding protein expressed during early neurogenesis, EMBO J. 10 (1991) 1135–1147.
[2] A. Mansouri, M. Hallonet, P. Gruss, Pax genes and their roles in cell differentiation and development, Curr. Opin. Cell Biol. 8 (1996) 851–857.
[3] N. Chi, J.A. Epstein, Getting your Pax straight: Pax proteins in development and disease, Trends Genet. 18 (2002) 41–47.
[4] D. Lang, J.A. Epstein, Sox10 and Pax3 physically interact to mediate activation of a conserved c-RET enhancer, Hum. Mol. Genet. 12 (2003) 937–945.
[5] J.A. Epstein, D.N. Shapiro, J. Cheng, P.Y. Lam, R.L. Maas, Pax3 modulates expression of the c-Met receptor during limb muscle development, Proc. Natl. Acad. Sci. USA 93 (1996) 4213–4218.
[6] A. Watanabe, K. Takeda, B. Ploplis, M. Tachibana, Epistatic relationship between Waardenburg syndrome genes MITF and PAX3, Nat. Genet. 18 (1998) 283–286.
[7] D.J. Epstein, M. Vekemans, P. Gros, Splotch (Sp2H), a mutation affecting development of the mouse neural tube, shows a deletion within the paired homeodomain of Pax-3, Cell 67 (1991) 767–774.
[8] D.J. Epstein, K.J. Vogan, D.G. Trasler, P. Gros, A mutation within intron 3 of the Pax-3 gene produces aberrantly spliced mRNA transcripts in the splotch (Sp) mouse mutant, Proc. Natl. Acad. Sci. USA 90 (1993) 532–536.
[9] G. Chalepakis, M. Goulding, A. Read, T. Strachan, P. Gruss, Molecular basis of splotch and Waardenburg Pax-3 mutations, Proc. Natl. Acad. Sci. USA 91 (1994) 3685–3689.
[10] S.J. Conway, D.J. Henderson, A.J. Copp, Pax3 is required for cardiac neural crest migration in the mouse: evidence from the splotch (Sp2H) mutant, Development 124 (1997) 505–514.
[11] M. Tassabehji, A.P. Read, V.E. Newton, R. Harris, R. Balling, P. Gruss, T. Strachan, Waardenburg's syndrome patients have mutations in the human homologue of the Pax-3 paired box gene, Nature 355 (1992) 635–636.
[12] C.T. Baldwin, C.F. Hoth, J.A. Amos, E.O. da-Silva, A. Milunsky, An exonic mutation in the HuP2 paired domain gene causes Waardenburg's syndrome, Nature 355 (1992) 637–638.
[13] M. Tassabehji, A.P. Read, V.E. Newton, M. Patton, P. Gruss, R. Harris, T. Strachan, Mutations in the PAX3 gene causing Waardenburg syndrome type 1 and type 2, Nat. Genet. 3 (1993) 26–30.
[14] F. Relaix, M. Polimeni, D. Rocancourt, C. Ponzetto, B.W. Schafer, M. Buckingham, The transcriptional activator PAX3-FKHR rescues the defects of Pax3 mutant mice but induces a myogenic gain-of-function phenotype with ligand-independent activation of Met signaling in vivo, Genes Dev. 17 (2003) 2950–2965.

[15] F.G. Barr, N. Galili, J. Holick, J.A. Biegel, G. Rovera, B.S. Emanuel, Rearrangement of the PAX3 paired box gene in the paediatric solid tumour alveolar rhabdomyosarcoma, Nat. Genet. 3 (1993) 113–117.
[16] N. Galili, R.J. Davis, W.J. Fredericks, S. Mukhopadhyay, F.J. Rauscher 3rd, B.S. Emanuel, G. Rovera, F.G. Barr, Fusion of a fork head domain gene to PAX3 in the solid tumour alveolar rhabdomyosarcoma, Nat. Genet. 5 (1993) 230–235.
[17] A.D. Hollenbach, J.E. Sublett, C.J. McPherson, G. Grosveld, The Pax3-FKHR oncoprotein is unresponsive to the Pax3-associated repressor hDaxx, EMBO J. 18 (1999) 3702–3711.
[18] O. Wiggan, A. Taniguchi-Sidle, P.A. Hamel, Interaction of the pRB-family proteins with factors containing paired-like homeodomains, Oncogene 16 (1998) 227–236.
[19] P. Magnaghi, C. Roberts, S. Lorain, M. Lipinski, P.J. Scambler, HIRA, a mammalian homologue of Saccharomyces cerevisiae transcriptional co-repressors, interacts with Pax3, Nat. Genet. 20 (1998) 74–77.
[20] D. Stamataki, M. Kastrinaki, B.S. Mankoo, V. Pachnis, D. Karagogeos, Homeodomain proteins Mox1 and Mox2 associate with Pax1 and Pax3 transcription factors, FEBS Lett. 499 (2001) 274–278.
[21] C. Murga, L. Laguinge, R. Wetzker, A. Cuadrado, J.S. Gutkind, Activation of Akt/protein kinase B by G protein-coupled receptors. A role for α and $\beta\gamma$ subunits of heterotrimeric G proteins acting through phosphatidylinositol-3-OH kinase γ, J. Biol. Chem. 273 (1998) 19080–19085.
[22] M. Murakami, K. Kataoka, S. Fukuhara, O. Nakagawa, H. Kurihara, Akt-dependent phosphorylation negatively regulates the transcriptional activity of dHAND by inhibiting the DNA binding activity, Eur. J. Biochem. 271 (2004) 3330–3339.
[23] M. Murakami, K. Kataoka, J. Tominaga, O. Nakagawa, H. Kurihara, Differential cooperation dHAND and three distinct E-proteins, Biochem. Biophys. Res. Commun. 323 (2004) 167–174.
[24] Y. Yamaguchi, T. Nagase, R. Makita, S. Fukuhara, T. Tomita, T. Tominaga, H. Kurihara, Y. Ouchi, Identification of multiple novel epididymis-specific beta-defencin isoforms in humans and mice, J. Immunol. 169 (2002) 2516–2523.
[25] E. Bober, T. Franz, H.H. Arnold, P. Gruss, P. Tremblay, Pax-3 is required for the development of limb muscles: a possible role for the migration of dermomyotomal muscle progenitor cells, Development 120 (1994) 603–612.
[26] M. Goulding, A. Lumsden, A.J. Paquette, Regulation of Pax-3 expression in the dermomyotome and its role in muscle development, Development 120 (1994) 957–971.
[27] F. Kanai, P.A. Marignani, D. Sarbassova, R. Yagi, R.A. Hall, M. Donowitz, A. Hisaminato, T. Fujiwara, Y. Ito, L.C. Cantley, M.B. Yaffe, TAZ: a novel transcriptional co-activator regulated by interactions with 14-3-3 and PDZ domain proteins, EMBO J. 19 (2000) 6778–6791.
[28] C.B. Cui, L.F. Cooper, X. Yang, G. Karsenty, I. Aukhil, Transcriptional coactivation of bone-specific transcription factor Cbfa1 by TAZ, Mol. Cell Biol. 23 (2003) 1004–1013.
[29] K.S. Park, J.A. Whitsett, T. Di Palma, J.H. Hong, M.B. Yaffe, M. Zannini, TAZ interacts with TTF-1 and regulates expression of surfactant protein-C, J. Biol. Chem. 279 (2004) 17384–17390.
[30] J.H. Hong, E.S. Hwang, M.T. McManus, A. Amsterdam, Y. Tian, R. Kalmukova, E. Mueller, T. Benjamin, B.M. Spiegelman, P.A. Sharp, N. Hopkins, M.B. Yaffe, TAZ, a transcriptional modulator of mesenchymal stem cell differentiation, Science 309 (2005) 1074–1078.

WFS1-deficiency increases endoplasmic reticulum stress, impairs cell cycle progression and triggers the apoptotic pathway specifically in pancreatic β-cells

Takahiro Yamada[1], Hisamitsu Ishihara[1*], Akira Tamura[1], Rui Takahashi[1], Suguru Yamaguchi[1], Daisuke Takei[1], Ai Tokita[1], Chihiro Satake[1], Fumi Tashiro[2], Hideki, Katagiri[3], Hiroyuki Aburatani[4], Jun-ichi Miyazaki[2] and Yoshitomo Oka[1]

[1]Division of Molecular Metabolism and Diabetes, Tohoku University Graduate School of Medicine, Sendai, Miyagi 980-8575, Japan. [2]Division of Stem Cell Regulation Research, Osaka University Graduate School of Medicine, Suita, Osaka 565-0871, Japan. [3]Division of Advanced Therapeutics for Metabolic Diseases, Tohoku University Graduate School of Medicine, Sendai, Miyagi 980-8575, Japan. [4]Genome Science Division, Research Center for Advanced Science and Technology, The University of Tokyo, Tokyo 153-8904, Japan.

Address correspondence to: Hisamitsu Ishihara, M.D., Ph.D.

Division of Molecular Metabolism and Diabetes, Tohoku University Graduate School of Medicine, 2-1 Seiryo-machi, Aoba-ku, Sendai, Miyagi 980-8575, Japan.

Tel. +81 22 717 7611, Fax. +81 22 717 7612.

E-mail, hisamitsu-ishihara@mail.tains.tohoku.ac.jp

SUMMARY

Wolfram syndrome, an autosomal recessive disorder associated with diabetes mellitus and optic atrophy, is caused by mutations in the *WFS1* gene encoding an endoplasmic reticulum (ER) membrane protein. Herein, we report that pancreatic islets of *wfs1*-deficient mice exhibit increases in phosphorylation of RNA-dependent protein kinase-like ER kinase, chaperone gene expressions and active XBP1 protein levels, indicating an enhanced ER stress response. We established *wfs1*-deficient MIN6 clonal β-cells by crossing *wfs1*-deficient mice with mice expressing simian virus 40 large T antigen in β-cells. These cells show essentially the same alterations in ER stress responses as *wfs1*-deficient islets, which were reversed by re-expression of WFS1 protein or overexpression of GRP78, a master regulator of the ER stress response. In contrast, these changes are not observed in heart, skeletal muscle, or brown adipose tissues with WFS1-deficiency. The increased ER stress response was accompanied by reduced BrdU incorporation and increased caspase-3 cleavage, indicating impaired cell cycle progression and accelerated apoptotic processes in the mutant islets. These changes are associated with increased expression of the cell cycle regulator $p21^{CIP1}$ in *wfs1*-deficient islets and clonal β-cells. Treatment of islets with thapsigargin, an ER stress inducer, caused upregulation of $p21^{CIP1}$. In addition, forced expression of $p21^{CIP1}$ resulted in reduced MIN6 β-cell numbers, suggesting the ER stress-induced increase in $p21^{CIP1}$ expression to be involved in β-cell loss in the mutant islets. These data indicate that WFS1-deficiency activates the ER stress response specifically in β-cells, causing β-cell loss through impaired cell cycle progression and increased apoptosis.

INTRODUCTION

Type 2 diabetes is caused by complex interactions between insulin resistance in peripheral tissues and impaired insulin secretion from pancreatic β-cells. There is a general consensus that the latter results from both impaired β-cell function and decreased β-cell mass (1-3). Adult β-cell mass is maintained by a balance between generation and death of β-cells. In patients with type 2 diabetes, new islet formation and β-cell replication are reportedly normal, and an increased rate of apoptosis has been suggested to underlie the loss of β-cell mass (4).

Recent studies using novel mutant mice have led to new insights into endoplasmic reticulum (ER) stress and maintenance of β-cell mass (5,6). The ER stress response, also known as the unfolded protein response (UPR), involves translational attenuation, transcriptional induction of chaperones and folding enzymes, as well as degradation of misfolded proteins, a process called ER-associated degradation (ERAD). When ER stress is strong and cellular survival mechanisms fail to correct the protein-folding defects, an ER stress-mediated apoptotic process is initiated (5-7). Mice with a homozygous null mutation of RNA-dependent protein kinase-like ER kinase (PERK) lose their ability to phosphorylate eukaryotic initiation factor 2α (eIF2α) and fail to attenuate translation in response to ER stress. These mice develop diabetes due to reduced β-cell mass (8). Importantly, mutations of the *EIF2AK3* gene encoding PERK in humans have been recognized as causing Wolcott-Rallison syndrome with diabetes mellitus in early infancy (9). A mouse model in which a Ser51Ala mutation of eIF2α prevents the protein from being phosphorylated by PERK and other eIF2α kinases, also displays a β-cell defect and impaired gluconeogenesis leading to lethal hypoglycemia

(10). Mice with a deletion mutation of $P58^{IPK}$, a cytosolic chaperone, were recently reported to exhibit β-cell failure and diabetes (11). These examples suggest that β-cells, producing large quantities of insulin and thus a greater load on the ER, are especially sensitive to ER stress.

Wolfram syndrome is a rare autosomal recessive disorder characterized by juvenile-onset diabetes mellitus, optic atrophy, diabetes insipidus and sensorineural deafness (12). This syndrome is caused by mutations in the *WFS1* gene (13,14), which encodes an ER resident membrane protein (15). Postmortem studies of the pancreas from subjects with Wolfram syndrome have shown β-cell loss (16). We recently established a line of mutant mice with a disrupted *wfs1* gene and found that these mice also exhibited impaired glucose homeostasis accompanied by a progressive reduction of β-cell mass (17). Thus, the *wfs1*-deficient mouse is a model for studying mechanisms of β-cell loss during the development of diabetes in Wolfram syndrome. We and others have also shown expression of WFS1 protein to be up-regulated by ER stress-inducing agents (18-20). A recent study employing IRE1α knockout and PERK knockout cells suggested that WFS1 is a component of the IRE1 and PERK signaling pathways (20). In addition, *wfs1*-deficient islets have been shown to exhibit increased DNA fragmentation in response to ER stress inducers (17), suggesting β-cell loss in Wolfram syndrome to be attributable to an inability to handle ER stress. A very recent study of islets conditionally lacking the *wfs1* gene in β-cells, demonstrated an increased GRP78 mRNA to GLUT2 mRNA ratio. This observation was interpreted as evidence of an enhanced ER stress response, on the assumption that GLUT2 mRNA levels represented the β-cell number in islets (21).

To further investigate the mechanisms underlying β-cell loss in Wolfram

syndrome, we conducted a systematic study of the UPR in *wfs1*-deficient islets as well as other tissues. We also created β-cell lines with WFS1-deficiency and studied UPR. We found all three UPR subpathways to be activated in *wfs1*-deficient islets and β-cell lines. Furthermore, we demonstrated increased cleavage of caspase-3, a hallmark of apoptosis, and impaired proliferation associated with enhanced expression of the cell cycle regulator $p21^{CIP1}$.

RESULTS

UPR activation in *wfs1*-deficient islets

A systematic study of the UPR was conducted using islets isolated from 6-week-old male *wfs1*-deficient mice with the B6 background. At 6 weeks of age, the β-cell mass of these mice begins to decrease (17). Accumulation of unfolded proteins in the ER is well known to induce dissociation of GRP78 from PERK, resulting in oligomerization and subsequent auto-phosphorylation of PERK. Activated PERK then phosphorylates eIF2α and suppresses general protein translation to reduce the ER load (5-7). In freshly isolated *wfs1*-deficient islets, PERK phosphorylation was increased (Fig. 1A). In addition, eIF2α phosphorylation was slightly but significantly enhanced with no alteration in total eIF2α levels in mutant islets (Fig. 1A). Thus, the ratio of phosphorylated eIF2α over total eIF2α levels analyzed by densitometry was increased by 27 ± 7% ($n = 4$ experiments, $p < 0.05$). These data indicate that one of three subpathways of the UPR arising from PERK phosphorylation is initiated in response to WFS1-deficiency in islets.

ER stress is also sensed by other ER resident proteins, IRE1 and ATF6, in addition to PERK (5-7). Activation of ATF6 via GRP78 dissociation and subsequent cleavage is known to induce the expressions of various chaperone genes, constituting another subpathway of the UPR (5-7). In *wfs1*-deficient islets, GRP94 mRNA levels were increased and those of GRP78 and $P58^{IPK}$ also tended to rise (Fig. 1B). Correspondingly, although the differences failed to reach statistical significance, levels of these chaperone proteins tended to be increased (Fig. 1C), suggesting that the ATF6 subpathway of the UPR is activated in response to WFS1-deficiency.